J Appl Electrochem (2014) 44:199–207
DOI 10.1007/s10800-013-0631-5

RESEARCH ARTICLE

Pt nanoparticles synthesized with new surfactants: improvement in C_1–C_3 alcohol oxidation catalytic activity

Fatih Şen · Gülsün Gökağaç

Received: 12 July 2013 / Accepted: 17 September 2013 / Published online: 29 September 2013

Abstract Platinum electrocatalysts were prepared using $PtCl_4$ as a starting material and 1-decylamine, *N*,*N*-dimethyldecylamine, 1-dodecylamine, *N*,*N*-dimethyldodecylamine, 1-hexadecylamine, and 1-octadecylamine as surfactants. These surfactants were used for the first time in this synthesis to determine whether the primary and/or tertiary structure and/or chain length of the surfactants, affects the size and/or activity of the catalysts in C_1–C_3 alcohol electro-oxidation reactions. Electrochemical measurements (cyclic voltammetry and chronoamperometry) indicated that the highest electrocatalytic performance was observed for the Pt nanocatalysts that were stabilized by *N*,*N*-dimethyldecylamine, and this has a tertiary amine structure with a short chain length ($R = C_{10}H_{21}$). The high performance may be due to the high electrochemical surface area, Pt(0)/Pt(IV) ratio, %Pt utility, and roughness factor (R_f). X-ray photoelectron spectroscopy, X-ray diffraction, atomic force microscopy, and transmission electron microscopy were used to determine the parameters that affect the catalytic activities.

Keywords Alcohol oxidation · Direct alcohol fuel cells · Platinum nanoparticles · Electrocatalysts · Carbon support

F. Şen (✉)
Biochemistry Department, Dumlupinar University, 43020 Kutahya, Turkey
e-mail: fatihsen1980@gmail.com; fatih.sen@dpu.edu.tr

G. Gökağaç (✉)
Chemistry Department, Middle East Technical University, 06531 Ankara, Turkey
e-mail: ggulsun@metu.edu.tr

1 Introduction

Fuel cells convert chemical energy directly into electrical energy with several advantages, such as simple construction, low cost, light weight, high efficiency, and low-pollution. Direct methanol fuel cells (DMFCs), which uses methanol directly as the fuel, are one of the promising fuel cell technologies due to their high energy density, relatively low operating temperature, absence of reformer unit, and the easy handling of methanol [1–4]. There has been considerable research effort directed towards methanol electro-oxidation [5, 6]. Apart from methanol, which is relatively toxic and volatile, other short chain organic alcohols such as ethanol, 1-propanol, and 2-propanol can also be used as a fuel [7, 8]. Ethanol is particularly interesting due to such advantages as renewability, safety, availability (from biomass products), and high energy density [9–11]. Therefore, ethanol may be more attractive than methanol for direct alcohol fuel cells. The complete oxidation of ethanol is not without problems such as the production of many adsorbed intermediates and by-products, and the difficulty in cleaving the C–C bond at low temperatures. C_3-alcohols, such as 1-propanol and 2-propanol, may also provide alternatives to methanol and ethanol [12–15]. Even though C_1–C_3 alcohols have a high energy content per unit mass, they do not exhibit any electrochemical activity, so a catalyst is needed to activate them. Platinum is a well-known electrocatalyst for the oxidation of alcohols on the anode of direct alcohol fuel cells (DAFCs) [16, 17]. The performance of the catalyst can be enhanced by using Pt nanoparticles instead of bulk Pt, due to their large surface area. Various surfactants can be used to produce stable platinum nanoparticles, and previous studies have shown that the surfactant can affect the size of metal particles and the catalytic performance of the catalysts [18]. In this study, six platinum nanoparticle catalysts have been

prepared using $PtCl_4$ as a starting material and 1-decylamine, *N*,*N*-dimethyldecylamine, 1-dodecylamine, *N*,*N*-dimethyldodecylamine, 1-hexadecylamine, and 1-octadecylamine as surfactants—for the first time. The size and activity of the catalysts towards C_1–C_3 alcohol oxidations, was measured in order to determine the effect of the chain length and the primary and tertiary structure of the surfactants. X-ray diffraction (XRD), X-ray photoelectron microscopy (XPS), atomic force microscopy (AFM), and transmission electron microscopy (TEM) were used to characterize the amine-stabilized platinum nanoparticles. Cyclic voltammetry (CV) and chronoamperometry (CA) measurements were performed to investigate the electrochemical activities and stabilities of all catalysts in the oxidation of methanol, ethanol, 1-propanol, and 2-propanol. Catalyst II, which was stabilized by the tertiary amine surfactant with the shortest chain length (*N*,*N*-dimethyldecylamine), is the most active catalyst. Its activity is 25.5, 49.6, 23.2, and 30.6 times higher for methanol, ethanol, 1-propanol, and 2-propanol oxidation reactions, respectively, than commercially available ETEK Pt catalysts.

2 Experimental

2.1 General

$PtCl_4$ (99 % Alfa Aesar), tetrahydrofuran (THF) (99.5 %, Merck), methanol (≥99.5 %, Merck), ethanol (99.9 %, Merck), 1-propanol (≥99.0 %, Merck), 2-propanol (≥99.5 %, Merck), and $HClO_4$ (60 %, Merck), lithium triethylborohydride (1.0 M dissolved in THF, Sigma Aldrich), 1-decylamine (Sigma Aldrich), *N*,*N*-dimethyldecylamine (Sigma Aldrich), 1-dodecylamine (Sigma Aldrich), *N*,*N*-dimethyldodecylamine (Sigma Aldrich), 1-hexadecylamine (Sigma Aldrich) and 1-octadecylamine (Sigma-Aldrich) and Carbon XC-72 (Cabot Europa Ltd.) were used as-received. Water was deionized by a Millipore water purification system (18 MΩ) analytical grade. All glassware and Teflon-coated magnetic stir bars were cleaned with aqua-regia before use, followed by washing with distilled water.

2.2 Instrumentation

The TEM micrographs of the catalysts were recorded using a JEOL 200 kV microscope. A drop of the Vulcan carbon–Pt nanoparticle solution was placed on 400-mesh carbon-coated copper grids and these were dried, under vacuum, at room temperature, before analysis. More than 300 particles were examined in order to obtain average particle size distributions of all prepared catalysts.

Specs spectrometer was used to perform XPS analyses using the Kα lines of Mg (1253.6 eV, 10 mA) as an X-ray source. A Cu double-sided tape (3 M Inc.) was used to deposit the samples. The C 1s line at 284.6 eV was chosen as a reference point and peak fittings were done using a Gaussian function.

A Rigaku diffractometer with an Ultima + theta–theta high-resolution goniometer, equipped with a Cu K_α source operating at 40 kV and 40 mA, was used to acquire XRD patterns of all samples. The scan range was 10°–90° and the scan rate was 5° min^{-1}.

A Digital Instruments Multi Mode AFM Nanoscope IV a (Veeco Ins., Santa Barbara, CA) was employed to visualize the surface topographies of the prepared catalysts at ambient temperature. It was operated in 'tapping' mode using 0.01–0.025 Ω cm antimony-doped silicon AFM probes (Ultrasharp TESP with about 2 nm tip radius curvature, cantilever spring constants of 20–80 N m^{-1} and resonance frequencies of 328–379 kHz). The images were analyzed using the Nanoscope 6.13 (version 6.13.r1, Veeco) software package. To prepare the AFM samples, 2.5 μL of the catalyst solution (diluting 300-fold or more with DI water) was placed directly on a freshly cleaved mica disk (supporting material) and allowed to dry in a vacuum at room temperature for at least 12 h.

All electrochemical experiments (CV and CA) were performed in a conventional three-electrode cell using a microcomputer-controlled potentiostat/galvanostat (Solartron 1285) at room temperature. The saturated calomel electrode (SCE), glassy carbon, and prepared catalysts served as the reference, counter, and working electrodes, respectively. The ink solutions on the working electrodes, including our nanocatalysts, were prepared as described in our previous study [18]. The amount of Pt in these ink solutions was determined by a Leeman Lab inductively coupled plasma spectroscope (ICP). The alcohol solutions that were used in these experiments, were fresh and unused, in order to obtain reproducible and reliable results.

2.3 Catalyst preparation

All of the prepared catalysts are shown in Table 1 and were prepared by an ethanol–superhydride reduction method. In this method, superhydride and ethanol are used to reduce a mixture of 0.25 mmol (0.0808 g) of $PtCl_4$ dissolved in small amount of anhydrous tetrahydrofuran and 0.25 mmol of surfactant. The observation of a brown color in the

Table 1 Catalysts and surfactants

	Surfactants
Catalyst I	1-Decylamine
Catalyst II	*N*,*N*-Dimethydecylamine
Catalyst III	1-Dodecylamine
Catalyst IV	*N*,*N*-Dimethyldodecylamine
Catalyst V	1-Hexadecylamine
Catalyst VI	1-Octadecylamine

solution indicates the formation of the amine-stabilized platinum nanoparticles. Excess surfactants are removed by washing with ethanol, followed by drying in a vacuum. The prepared platinum nanoparticles and carbon XC-72, in a 1:10 ratio, were vigorously mixed in ethanol for 2 days. It was dried under vacuum at room temperature.

3 Results and discussion

3.1 XRD, AFM, and TEM characterization of the prepared catalysts

All the prepared catalysts were characterized by XRD; this indicates the crystalline structure, orientation, lattice constants, and crystallite sizes. The X-ray patterns for our Pt catalysts are shown in Fig. 1. The diffraction peaks at $2\theta = 39.90$, 46.60, 67.50, and 81.20 can be attributed to the (*111*), (*200*), (*220*), and (*311*) planes of the face-centered cubic (fcc) crystal lattice of platinum. The lattice parameter (a_{Pt}) value of the prepared catalysts was calculated as 3.922 Å using the Pt (*220*) diffraction peak from the following equation [19]

$$\sin\theta = \frac{\lambda\sqrt{h^2+k^2+l^2}}{2a} \quad \text{(for a cubic structure)}$$

where h, k, and l are adjacent lattice planes, θ is the angle at the position of peak maximum, λ = the wavelength of X-ray used (1.54056 Å), and a is lattice parameter. The average crystallite sizes of the catalysts I, II, III, IV, V, and VI were calculated as 3.20, 3.40, 3.03, 3.25, 2.86, and 2.59 nm, respectively, using the full width half-maximum of the (*220*) peaks in the Scherrer equation [20]:

$$d(\text{Å}) = \frac{k\lambda}{\beta\cos\theta}$$

where k = a coefficient (0.9), λ = the wavelength of the X-ray used (1.54056 Å), β = the full width half-maximum of respective diffraction peak (rad), and θ = the angle at the position of peak maximum (rad). These data indicate that as the chain length of surfactant increases, the size of platinum crystallites decreases, which is in good agreement with previous studies [21–23]. Additionally, the size of the platinum crystallites that were prepared by tertiary amine surfactants is larger.

The particle size distributions and atomic lattice fringes of the prepared catalysts were analyzed using high-resolution electron microscopy (HRTEM). The electron

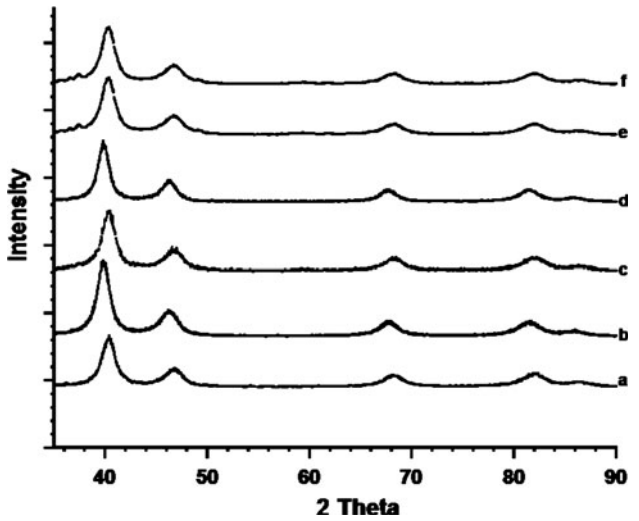

Fig. 1 XRD patterns of catalysts I (*a*), II (*b*), III (*c*), IV (*d*), V (*e*), and VI (*f*)

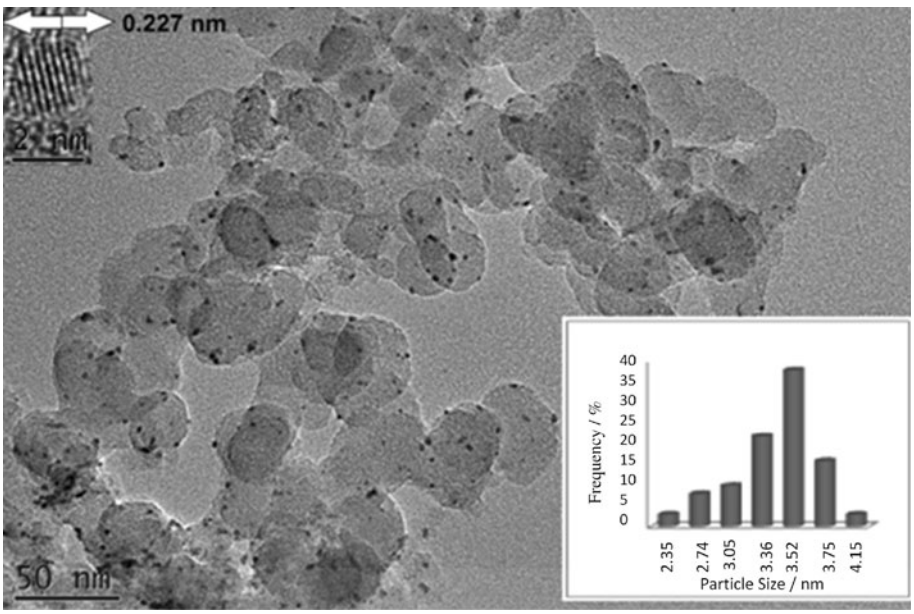

Fig. 2 High-resolution transition electron micrograph and particle size histogram of catalyst II

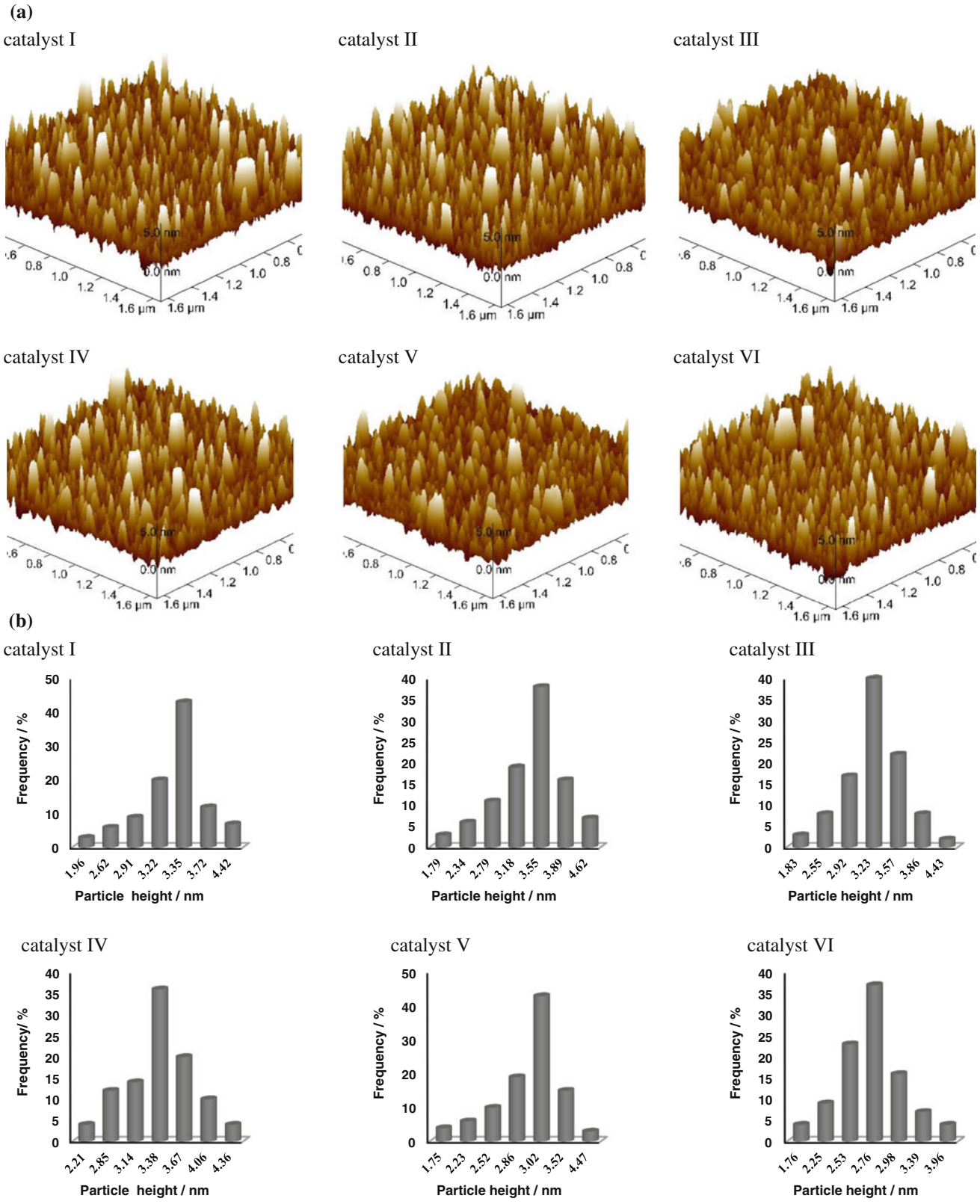

Fig. 3 **a** AFM images of catalysts. **b** Histogram of the height of the particles obtained from the AFM data. **c** Histogram of the lateral diameter of the particles obtained from the AFM data

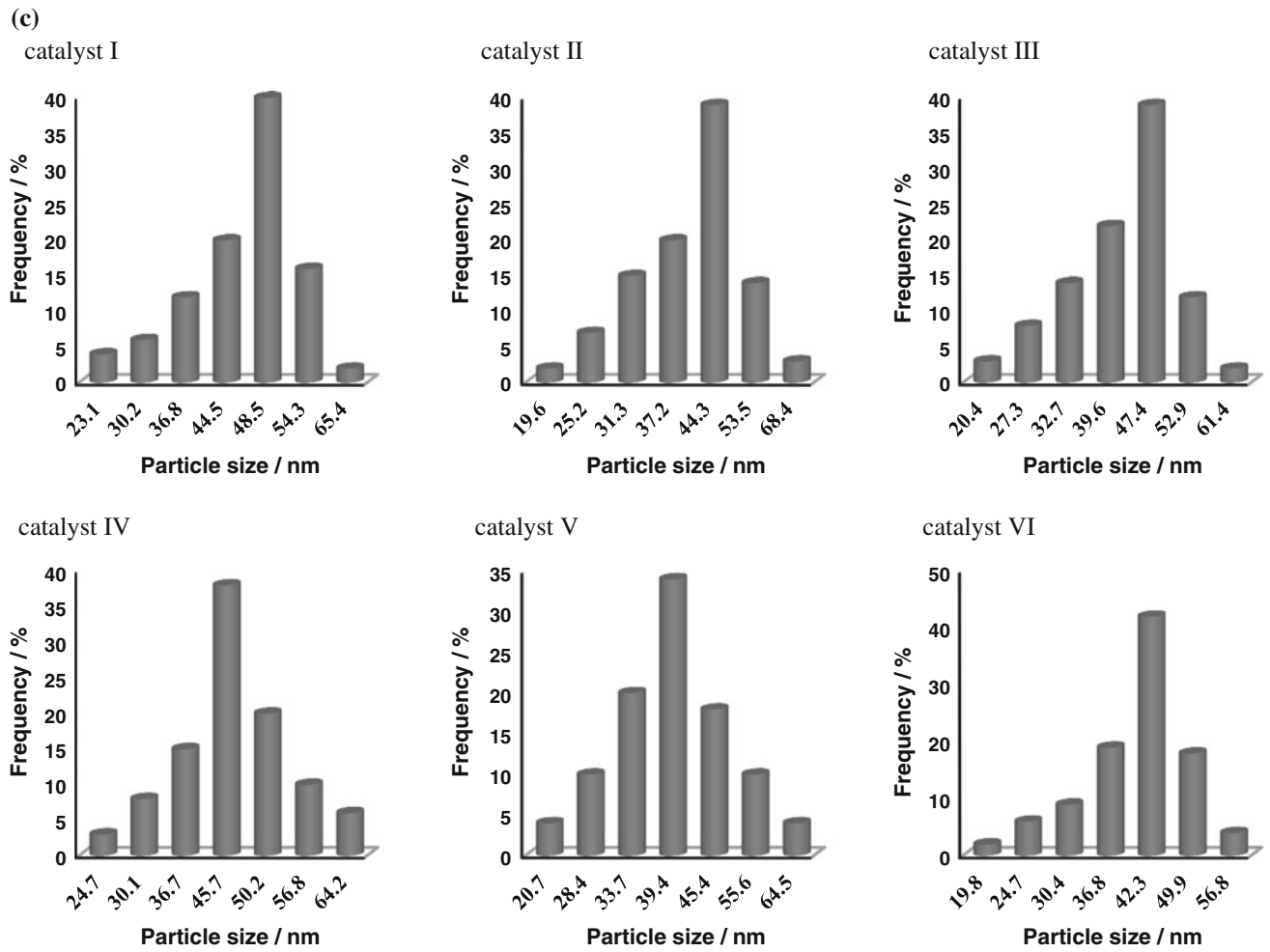

Fig. 3 continued

Table 2 Average crystallite platinum particles size determined by (a) X-ray line broadening, (b) transmission electron microscopy, (c) particle height, (d) observed lateral diameter, and (e) deconvoluted lateral diameter determined by AFM

	a (nm)	b (nm)	c (nm)	d (nm)	e (nm)	e c^{-1}
Catalyst I	~3.20 ± 0.36	~3.30 ± 0.85	~3.35 ± 0.44	~48.5 ± 8.03	37.3	11.1
Catalyst II	~3.40 ± 0.41	~3.52 ± 0.70	~3.55 ± 0.58	~44.3 ± 9.30	34.1	9.6
Catalyst III	~3.03 ± 0.32	~3.10 ± 0.82	~3.23 ± 0.43	~47.4 ± 8.69	36.5	11.3
Catalyst IV	~3.25 ± 0.37	~3.33 ± 0.92	~3.38 ± 0.44	~45.7 ± 8.93	35.1	10.4
Catalyst V	~2.86 ± 0.21	~3.00 ± 0.96	~3.02 ± 0.46	~45.4 ± 9.26	34.9	11.6
Catalyst VI	~2.59 ± 0.20	~2.70 ± 0.84	~2.76 ± 0.40	~42.3 ± 7.86	32.5	11.8

micrograph and particle size histogram for catalyst II is shown in Fig. 2. The platinum nanoparticles are uniformly distributed on the carbon support and the average particle sizes were found to be ~3.30 ± 0.85, ~3.52 ± 0.70, ~3.10 ± 0.82, 3.33 ± 0.92, 3.00 ± 0.96, and ~2.70 ± 0.84 nm for catalysts I, II, III, IV, V, and VI, respectively. These results are in good agreement with the XRD data. Occasionally, a small number of large particles, ~50–100 nm in diameter, are observed. This is most probably due to the accumulation of the smaller individual particles. Atomic lattice fringes were also examined for all catalysts, e.g., left inset of Fig. 2. The spacing for the Pt (111) planes was found to be 0.227 nm, which is very close to nominal Pt (111) spacing of 0.228 nm [24, 25].

These catalysts were also analyzed by AFM to obtain height and lateral diameter distributions of the Pt nanoparticles. The AFM images, height, and lateral diameter distributions, for our catalysts are shown in Fig. 3a–c, respectively. The height of the particles are 3.35, 3.55, 3.23, 3.38, 3.02, and 2.76 nm for catalysts I, II, III, IV, V, and VI, respectively. The height of the particles of our catalysts is in good agreement with XRD and TEM results (Table 2). The lateral diameter of the Pt nanoparticles was found to be 48.5, 44.3, 47.4, 45.7, 45.4, and 42.3 nm for catalysts I, II, III, IV, V, and VI, respectively. These results are very different from the particle size determined by XRD or TEM and are most probably due to tip contamination and/or tip convolution. Tip deconvolution was calculated to try to improve the AFM lateral diameter data with the assistance of a deconvolution formula given below [26, 27]. The mean half angle of the tip, 17°θ, instead of the apex radius, is used because of the larger lateral dimensions of the particles compared to the tip radius.

$$r_c = r\left[\cos\theta + \left(\cos^2\theta + (1+\sin\theta)\right.\right.$$
$$\left.\left.\times\left(-1+(\tan\theta/\cos\theta)+\tan^2\theta\right)\right)^{1/2}\right],$$

where r and r_c are the real particle diameter and the observed particle diameter, respectively.

The deconvoluted lateral size of the particles is 37.3, 34.1, 36.5, 35.1, 34.9, and 32.5 nm for catalysts I, II, III, IV, V, and VI, respectively (Table 2). The large value of the ratio of deconvoluted lateral size to height (e c^{-1}) may be associated to the aggregation of particles on the freshly cleaved smooth mica surface owing to capillary forces, and/or tip indentation.

3.2 XPS characterization of the prepared catalysts

The effects of the oxidation state of platinum on the catalytic activity of the prepared catalysts, was probed using XPS. For this purpose, the Pt 4f region of the spectrum was fitted using a Gaussian–Lorentzian method after background subtraction using Shirley's method [28] and analyzed in terms of relative peak area and chemical shift of Pt. The Pt 4f spectra of the catalysts are shown in Fig. 4 and each spectrum consists of two pairs of doublets. The ratio of the $4f_{7/2}$ to $4f_{5/2}$ signals for all catalysts was 4:3, which is in good agreement with the literature [28, 29]. The more intense doublet at about 71.0 and 74.3 eV is a signature of metallic platinum [30, 31] and the other doublet at about 74.3 and 77.6 eV is most likely caused by a Pt(IV) species such as PtO_2 and/or $Pt(OH)_4$ [32–36] on the surface as shown in Table 3. The ratios of Pt (0) to Pt(IV) for the prepared catalysts were calculated from the relative peak area of the Pt 4f spectrum. Catalyst II has the highest metallic character (the ratio of Pt(0) to Pt(IV) is highest) potentially providing a higher electrochemical active area and improved catalytic performance. The Pt(0) peak position is also important in defining the metallic character of the platinum, i.e., the lower the binding energy of Pt(0) the higher the metallic character of platinum. Catalyst II therefore has the highest metallic character as it has the lowest Pt 4f peak position (70.7 eV).

3.3 Electrochemical activity of the prepared catalysts

The cyclic voltammogram of catalyst I, in 0.1 M $HClO_4$, showing typical hydrogen and oxygen adsorption/desorption regions is shown in Fig. 5. The cyclic voltammograms of the other catalysts are very similar. The electrochemical active surface areas (ECSA) of the catalysts were also measured in 0.1 M $HClO_4$ using the hydrogen desorption region, under an Ar atmosphere—before and during the measurement—to deaerate the electrolyte [37]. The ECSA (m^2 g^{-1}) were calculated using following formula:

$$\text{ECSA} = \frac{Q\ (\text{mC})}{\text{Pt loading on electrode} \times 0.21\ \text{mC cm}^{-2}}$$

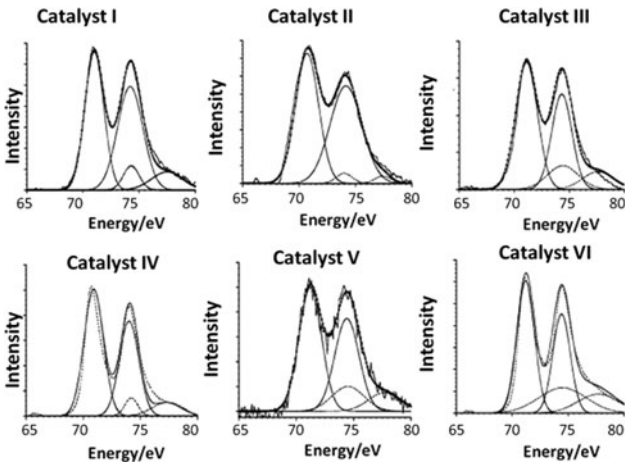

Fig. 4 Pt 4f electron spectra of all catalysts

Table 3 Pt $4f_{7/2}$ core binding energies, eV, of the prepared catalysts

	Pt $4f_{7/2}$ Pt(0)	Pt $4f_{7/2}$ Pt(IV)	Pt(0) $Pt(IV)^{-1}$
Catalyst I	71.0 (84.5)	74.3 (15.5)	5.45
Catalyst II	70.7 (95.6)	74.1 (4.4)	21.73
Catalyst III	71.1 (78.8)	74.4 (21.2)	3.72
Catalyst IV	70.9 (87.2)	74.0 (12.8)	6.81
Catalyst V	71.2 (74.7)	74.4 (25.3)	2.95
Catalyst VI	71.3 (67.0)	73.9 (33.0)	2.03

The numbers in parentheses are the relative intensities of the species

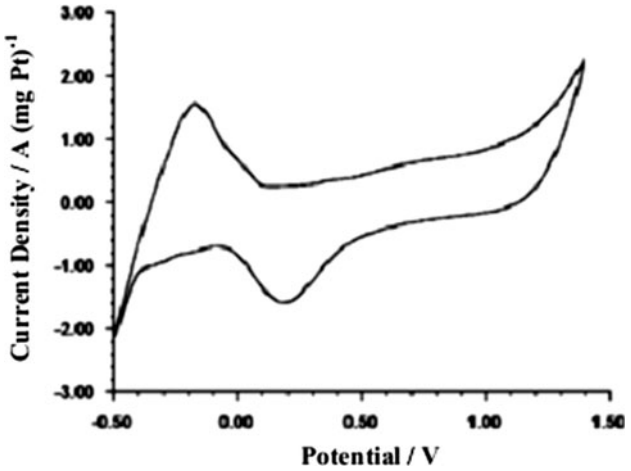

Fig. 5 Cyclic voltammogram of catalyst I in 0.1 M $HClO_4$ at room temperature. Scan rate is 50 mV s^{-1}

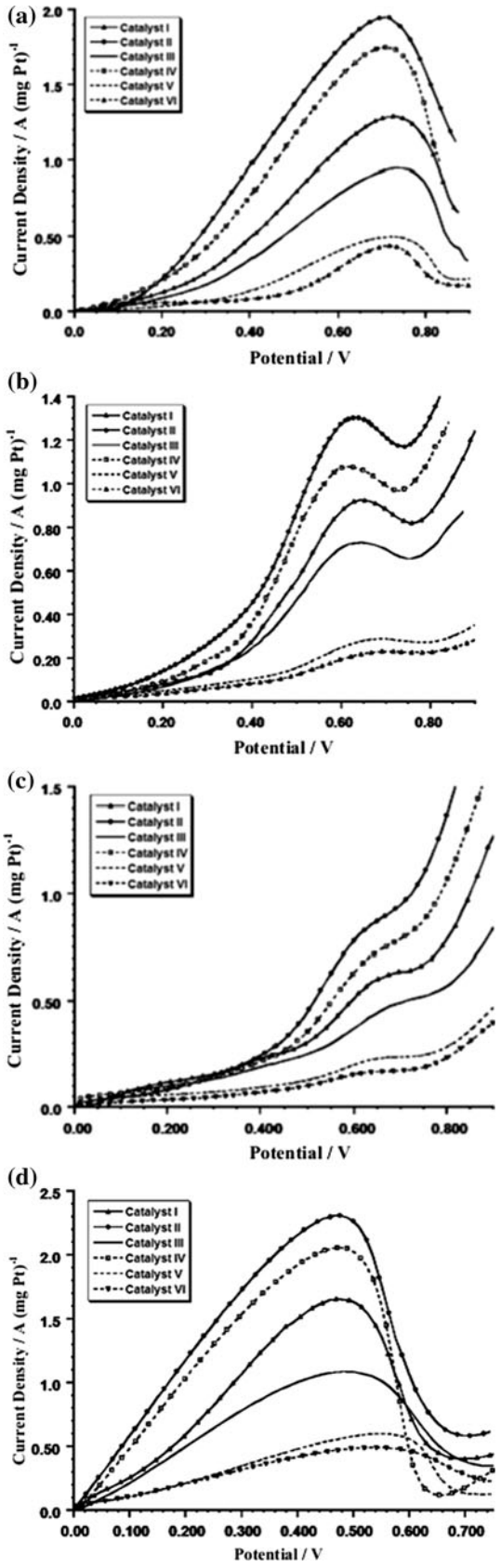

Fig. 6 **a** Anodic part of the cyclic voltammogram of the catalysts in 0.1 M $HClO_4$ + 0.5 M CH_3OH at room temperature. Scan rate is 50 mV s^{-1}. **b** Anodic part of the cyclic voltammogram of the catalysts in 0.1 M $HClO_4$ + 0.5 M CH_3CH_2OH at room temperature. Scan rate is 50 mV s^{-1} **c** Anodic part of the cyclic voltammogram of the catalysts in 0.1 M $HClO_4$ + 0.5 M 1-propanol at room temperature. Scan rate is 50 mV s^{-1}. **d** Anodic part of the cyclic voltammogram of the catalysts in 0.1 M $HClO_4$ + 0.5 M 2-propanol at room temperature. Scan rate is 50 mV s^{-1}

where Q is the electric charge for hydrogen desorption, and assumes a correspondence value of 0.21 mC cm^{-2} Pt, which indicates the charge required to oxidize a monolayer of H_2 on platinum. The chemical surface areas (CSA) of these nanocatalysts were calculated using the following formula:

$$\mathrm{CSA} = \frac{6 \times 10^3}{\rho \times d}$$

where d is the mean Pt crystalline size in Å (from the XRD results) and ρ is the density of Pt metal (21.4 g cm^{-2}) [38].

Table 4 The comparisons of particle size, ECSA, CSA, and Pt utilization for all prepared catalysts and a commercial Pt catalyst

	Particle size (nm)	ECSA (m^2 g^{-1})	Roughness factor R_f	CSA (m^2 g^{-1})	Pt utility (%)
Catalyst I	~3.20	76.56	156.2	87.62	87.38
Catalyst II	~3.40	79.36	162.0	82.46	96.24
Catalyst III	~3.03	73.60	150.2	92.53	79.54
Catalyst IV	~3.25	77.74	158.7	86.27	90.11
Catalyst V	~2.86	61.02	124.5	98.03	62.25
Catalyst VI	~2.69	57.95	118.3	104.2	55.61
Pt (ETEK)	2.70	50.60	103.3	103.0	49.10

Table 5 The anodic peak potential and maximum currents for all prepared catalysts in methanol, ethanol, 1-propanol, and 2-propanol

Alcohol	Catalyst I	Catalyst II	Catalyst III	Catalyst IV	Catalyst V	Catalyst VI
Methanol	1.26 A (mg Pt)$^{-1}$ at 0.73 V	1.95 A (mg Pt)$^{-1}$ at 0.68 V	0.90 A (mg Pt)$^{-1}$ at 0.75 V	1.75 A (mg Pt)$^{-1}$ at 0.69 V	0.40 A (mg Pt)$^{-1}$ at 0.76 V	0.35 A (mg Pt)$^{-1}$ at 0.74 V
Ethanol	0.88 A (mg Pt)$^{-1}$ at 0.66 V	1.30 A (mg Pt)$^{-1}$ at 0.65 V	0.74 A (mg Pt)$^{-1}$ at 0.64 V	1.08 A (mg Pt)$^{-1}$ at 0.63 V	0.26 A (mg Pt)$^{-1}$ at 0.67 V	0.20 A (mg Pt)$^{-1}$ at 0.68 V
1-Propanol	0.63 A (mg Pt)$^{-1}$ at 0.65 V	0.82 A (mg Pt)$^{-1}$ at 0.62 V	0.46 A (mg Pt)$^{-1}$ at 0.68 V	0.71 A (mg Pt)$^{-1}$ at 0.64 V	0.21 A (mg Pt)$^{-1}$ at 0.65 V	0.17 A (mg Pt)$^{-1}$ at 0.66 V
2-Propanol	1.66 A (mg Pt)$^{-1}$ at 0.48 V	2.35 A (mg Pt)$^{-1}$ at 0.45 V	1.02 A (mg Pt)$^{-1}$ at 0.50 V	2.04 A (mg Pt)$^{-1}$ at 0.46 V	0.54 A (mg Pt)$^{-1}$ at 0.56 V	0.48 A (mg Pt)$^{-1}$ at 0.54 V

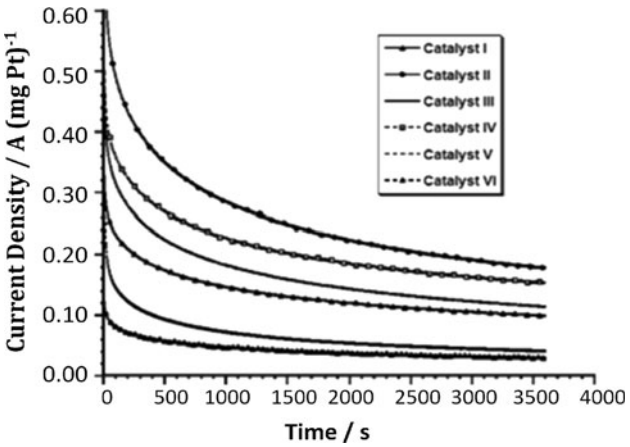

Fig. 7 Chronoamperometric curves of all prepared catalysts towards the methanol oxidation at 0.6 V (vs. SCE) in 0.1 M $HClO_4$ + 0.5 M CH_3OH

Pt utilization efficiency of the catalysts is calculated using ECSA and CSA (% Pt utility = (ECSA/CSA) × 100) and all these data are shown in Table 4. In addition, the roughness factor, R_f (m^2 g^{-1} Pt cm^{-2}), of all catalysts was calculated by using the real ECSA and the geometric area A_g (cm^2) [39] as in the following formula:

$$R_f = \frac{\text{ECSA}}{A_g}$$

From Table 4 it can be seen that in terms of ECSA, % Pt efficiency and R_f values catalyst II > IV > I > III > V > VI. In other words, catalyst II has the highest active surface area, % Pt utility, and roughness factor, which gives an indication that it may have the highest catalytic performance.

When methanol, ethanol, 1-propanol, or 2-propanol was added to the 0.1 M $HClO_4$ electrolyte solution the classical alcohol oxidation response was observed for all catalysts. Only the anodic parts of the CV are shown in Fig. 6a–d. The CV results indicate that catalyst II (stabilized by the tertiary amine with the shortest chain length surfactant, *N*,*N*-dimethyldecylamine) has the highest catalytic performance: ~1.95 A (mg Pt)$^{-1}$ at 0.68 V for methanol, ~1.30 A (mg Pt)$^{-1}$ at 0.65 V for ethanol, 0.82 A (mg Pt)$^{-1}$ at 0.62 V for 1-propanol and 2.35 A (mg Pt)$^{-1}$ at 0.45 V for 2-propanol (Table 5). The enhancement of the catalytic performance of this catalyst, compared to commercially available ETEK Pt catalyst, is 25.5, 49.6, 23.2, and 30.6 times with regards to the methanol, ethanol, 1-propanol, and 2-propanol oxidation reactions, respectively [40–46]. This highest catalytic performance can be explained high: Pt(0) to Pt(IV) ratio, ECSA, percent platinum utility, and roughness factor.

CA techniques were utilized in order to investigate the long-term stability of catalysts in the C_1–C_3 alcohol oxidations. The measurements were done at a potential of 0.6 V (vs. SCE) for 3600 s. Figure 7 shows the curves for the methanol oxidation reaction and is representative of the other alcohol oxidations. A rapid current decay was observed which indicates the poisoning of the electrocatalysts. Nevertheless, the CA results indicate that all catalysts have long-term stability, and catalyst II was found to be the most stable due to its higher oxidation current after a 3600 s; this is consistent with the CV data.

4 Conclusion

Carbon-supported platinum nanoparticle catalysts were synthesized, characterized and their catalytic activity towards C_1–C_3 alcohol oxidation determined. The surfactants 1-decylamine, *N*,*N*-dimethyldecylamine, 1-dodecylamine, *N*,*N*-dimethyldodecylamine, 1-hexadecylamine, 1-octadecylamine were used, for the first time, in the synthesis of these catalysts. The data indicates that the catalyst which is stabilized by a tertiary amine with a shorter chain is larger in size and has increased catalytic activity, i.e., catalyst II (*N*,*N*-dimethyldecylamine). This is most probably due to the high ECSA, percent platinum utility, roughness factor, and Pt(0) to Pt(IV) ratio. This most active catalyst (catalyst II) has activities of 25.5, 49.6, 23.2, and 30.6 times higher, than the commercially available catalyst, towards methanol, ethanol, 1-propanol, and 2-propanol oxidation reactions, respectively.

Acknowledgments The authors gratefully acknowledge TÜBİTAK (Türkiye Bilimsel ve Teknik Araştırma Kurumu, Grant 111T162) for financial support and the Central Laboratory of the Middle East Technical University for acquiring XPS, TEM, and elemental analyses. The authors also thank Dr. Michael W. Pitcher for editing and proofreading this manuscript.

References

1. Costamagna P, Srinivasan S (2001) J Power Sources 102:242–252
2. Ren X, Zelenay P, Thomas A, Davey J, Gottesfeld S (2000) J Power Sources 86:111
3. Wasmus S, Kuver A (2000) Electrochim Acta 45:4319
4. Reddington E, Sapienza A, Gurau B, Viswanathan R, Sarangapani S, Smotkin ES, Mallouk TE (1998) Science 280:1735
5. Sumodjo PTA, Silva EJ, Rabochai T (1989) J Electroanal Chem 271:305
6. Kabbabi A, Faure R, Durand R, Beden B, Hahn F, Leger J-M, Lamy C (1998) J Electroanal Chem 444:41–53
7. Rodrigues IA, De Souza JPI, Pastor E, Nart FC (1997) Langmuir 13:6829
8. Delime F, Leger J-M, Lamy C (1999) J Appl Electrochem 29:1249
9. Datta J, Sıngh S, Das S, Bandyopadhyay NR (2009) Bull Mater Sci 32(6):643
10. Zhou WJ, Song SQ, Li WZ, Zhou ZH, Sun GQ, Xin Q, Douvartzides S, Tsiakaras P (2005) J Power Sources 140:50
11. Lamy C, Belgsir EM, Leger JM (2001) J Appl Electrochem 31:799
12. Qi Z, Kaufman A (2002) J Power Sources 112:121–129
13. Cao D, Bergens SH (2003) J Power Sources 124:12–17
14. Qi Z, Hollett M, Attia A, Kaufman A (2002) Electrochem Solid-State Lett 5:A129–A130
15. Cao D, Bergens SH (2003) J Power Sources 124:12–17
16. Wei ZD, Li L, Luo YH, Yan C, Sun CX, Yin GZ, Shen PK (2006) J Phys Chem B 110:26055
17. Rodrigues IA, De Souza JPI, Pastor E, Nart FC (1997) Langmuir 13:6829
18. Şen F, Gökağaç G (2007) J Phys Chem C 111:1467–1473
19. Liu Z, Ling XY, Su X, Lee JY (2004) J Phys Chem B 108:8234–8240
20. Klug H, Alexander L (1954) X-ray diffraction procedures, 1st edn. Wiley, New York
21. Kawasaki H, Uota M, Yoshimura T, Fujikawa D, Sakai G, Kijima T (2006) J Colloid Interface Sci 300:149–154
22. Prabhuram J, Wang X, Hui CL, Hsing I-M (2003) J Phys Chem B 107:11057–11064
23. Şen F, Gökağaç G (2007) J Phys Chem C 111:1467–1473
24. Yonezawa T, Toshima N, Wakai C, Nakahara M, Nishinaka M, Tominaga T, Nomura H (2000) Colloids Surf A 169:35–45
25. Liang L, Sun G, Sun S, Liu J, Tang S, Li H, Zhou B, Xin Q (2005) Electrochim Acta 50:5384–5389
26. Sen F, Sen S, Gokagac G (2011) Phys Chem Chem Phys 13(4):1676–1684
27. Liu Z, Yu C, Russakova IA, Huang D, Strasser P (2008) Top Catal 49:241–250
28. Huang J, Yang H, Huang Q, Tang Y, Lu T, Akins DL (2004) J Electrochem Soc 151:A1810
29. Kennedy BJ, Hamnett A (1990) J Electroanal Chem 283:271
30. Sen F, Gokagac G (2007) J Phys Chem C 111(15):5715–5720
31. Deivaraj TC, Chen WX, Lee JY (2003) J Mater Chem 13:2555
32. Watanabe M, Uchida M, Motoo S (1987) J Electroanal Chem 229:395–406
33. Goodenough JB, Hamnett A, Kennedy BJ, Manoharan R, Weeks SA (1988) J Electroanal Chem 240:133–145
34. Gökağaç G, Kennedy BJ, Cashion JD, Brown LJ (1993) J Chem Soc, Faraday Trans 89:151–157
35. Peuckert M (1984) Electrochim Acta 29(10):1315–1320
36. Peuckert M, Bonzel HP (1984) Surf Sci 145(1):239–259
37. Liu ZL, Lee JY, Han M, Chen WX, Gan LM (2002) J Mater Chem 12:2453
38. Wang ZB, Yin GP, Shi PF (2005) J Electrochem Soc 152:A2406–A2412
39. Sen Gupta S, Datta J (2005) J Chem Sci 117:337–344
40. Kim YT, Mitani T (2006) J Catal 238:394–401
41. Kadirgan F, Beyhan S, Atilan T (2009) Int J Hydrogen Energy 34(10):4312–4320
42. Watanabe M, Uchida M, Motoo S (1987) J Electroanal Chem 229:395
43. Otomo J, Li X, Kobayashi T, Wen C-J, Nagamoto H, Takahashi H (2004) J Electroanal Chem 573:99
44. Ozturk Z, Sen F, Sen S, Gokagac G (2012) J Mater Sci 47:8134–8144
45. Ertan S, Sen F, Sen S, Gokagac G (2012) J Nanopart Res 14:922–926
46. Sen F, Gokagac G, Sen S (2013) J Nanopart Res. doi:10.1007/s11051-013-1979-5